Molecular near-field antenna effect in resonance hyper-Raman scattering: Intermolecular vibronic intensity borrowing of solvent from solute through dipole-dipole and dipole-quadrupole interactions

Rintaro Shimada and Hiro-o Hamaguchi

Citation: The Journal of Chemical Physics **140**, 204506 (2014); doi: 10.1063/1.4879058
View online: http://dx.doi.org/10.1063/1.4879058
View Table of Contents: http://scitation.aip.org/content/aip/journal/jcp/140/20?ver=pdfcov
Published by the AIP Publishing

Molecular near-field antenna effect in resonance hyper-Raman scattering: Intermolecular vibronic intensity borrowing of solvent from solute through dipole-dipole and dipole-quadrupole interactions

Rintaro Shimada[a] and Hiro-o Hamaguchi[a),b)]
Department of Applied Chemistry and Institute of Molecular Science, National Chiao Tung University, 1001 University Road, Hsinchu 30010, Taiwan

(Received 26 February 2014; accepted 8 May 2014; published online 28 May 2014)

We quantitatively interpret the recently discovered intriguing phenomenon related to resonance Hyper-Raman (HR) scattering. In resonance HR spectra of all-*trans*-β-carotene (β-carotene) in solution, vibrations of proximate solvent molecules are observed concomitantly with the solute β-carotene HR bands. It has been shown that these solvent bands are subject to marked intensity enhancements by more than 5 orders of magnitude under the presence of β-carotene. We have called this phenomenon the molecular-near field effect. Resonance HR spectra of β-carotene in benzene, deuterated benzene, cyclohexane, and deuterated cyclohexane have been measured precisely for a quantitative analysis of this effect. The assignments of the observed peaks are made by referring to the infrared, Raman, and HR spectra of neat solvents. It has been revealed that infrared active and some Raman active vibrations are active in the HR molecular near-field effect. The observed spectra in the form of difference spectra (between benzene/deuterated benzene and cyclohexane/deuterated cyclohexane) are quantitatively analyzed on the basis of the extended vibronic theory of resonance HR scattering. The theory incorporates the coupling of excited electronic states of β-carotene with the vibrations of a proximate solvent molecule through solute–solvent dipole–dipole and dipole–quadrupole interactions. It is shown that the infrared active modes arise from the dipole–dipole interaction, whereas Raman active modes from the dipole–quadrupole interaction. It is also shown that vibrations that give strongly polarized Raman bands are weak in the HR molecular near-field effect. The observed solvent HR spectra are simulated with the help of quantum chemical calculations for various orientations and distances of a solvent molecule with respect to the solute. The observed spectra are best simulated with random orientations of the solvent molecule at an intermolecular distance of 10 Å. © *2014 AIP Publishing LLC*. [http://dx.doi.org/10.1063/1.4879058]

I. INTRODUCTION

Hyper-Raman (HR) scattering is one of the nonlinear analogues of Raman scattering that provides molecular vibrational spectra with unique selection and polarization rules.[1–11] Recently, we discovered and reported a new phenomenon in resonance HR scattering of all-*trans*-β-carotene (hereafter abbreviated as β-carotene) in organic solvents.[12] Certain solvent HR bands were found to gain intensities by more than 5 orders of magnitude in the presence of β-carotene. No solvent HR bands were observed from neat solvents without β-carotene under exactly the same experimental conditions. This phenomenon was interpreted in terms of intermolecular vibronic coupling in which solute (β-carotene) electronic states interact with vibrations of neighboring solvent molecules.[13] We called it the molecular near-field effect[12] in analogy with near-field Raman scattering like Surface Enhanced Raman Scattering (SERS) and Tip Enhanced Raman Scattering (TERS), in which molecules in the vicinity of a photo-excited small metal structure are subject to giant Raman intensity enhancements ascribed to the local excitations of electrons.

We proposed an extended vibronic theory incorporating solute/solvent intermolecular vibronic coupling and accounted for the observed HR intensity enhancement as intermolecular vibronic intensity borrowing.[13,14] However, the origin of solute/solvent vibronic coupling was not discussed in these previous papers with coupling constants introduced in a purely phenomenological manner. The selection rules as well as orientation dependence of the effect were not elucidated either.

In the present paper, we develop our vibronic theory to discuss in further details of the intermolecular vibronic interaction and elucidate the physical origin of the molecular near-field effect in resonance HR scattering. High signal to noise ratio (S/N) experimental data for benzene and cyclohexane in the forms of difference spectra (C_6H_6–C_6D_6 for benzene and C_6H_{12}–C_6D_{12} for cyclohexane) are used in order to eliminate the background signals due to HR signal of solute as well as two-photon excited fluorescence. Thanks to the high symmetry of benzene and cyclohexane, clear selection rules are derived experimentally by comparing the observed HR spectra with the already well-established band

[a)] A part of this research was performed while R. Shimada and H. Hamaguchi were at Department of Chemistry, the University of Tokyo, 7-3-1 Hongo, Bunkyo-ku, Tokyo 113-0033, Japan.
[b)] Author to whom correspondence should be addressed. Electronic mail: hhama@nctu.edu.tw

assignments.[15–18] These selection rules are well accounted for in terms of solute/solvent electrostatic multipole interactions, namely, dipole–dipole and dipole–quadrupole interactions. The orientation dependence of the enhanced solvent HR spectra is then theoretically calculated. The calculation shows that the observed solvent HR spectra are best reproduced by assuming random orientations of the solute molecules around β-carotene. The mechanism of resonance HR molecular near-field effect is thus clearly identified as vibronic intensity borrowing due to the solute/solvent dipole–dipole and dipole–quadrupole interactions.

II. THEORY

In previous papers,[13,14] we extended the vibronic theory of resonance HR scattering[10,11,19–22] to incorporate an intermolecular vibronic coupling term in a phenomenological manner. Now the theory is further developed to a more rigorous form in which solvent molecular states are explicitly taken into account.

A. Intermolecular vibronic coupling

Consider a bimolecular system where a solute (labeled by A) and a solvent molecule (labeled by B) are weakly coupled. Here, we assume that the solute has multiple low lying excited electronic states that may be in resonance with the incident/scattered electromagnetic field, whereas the solvent (ordinary organic solvent) is completely off from electronic resonances.

In the absence of overlap of the molecular electronic wave functions, a zero-order electronic state of the bimolecular system can be expressed as a product of the solute and solvent electronic states. Suppose we have a zero-order total excited electronic state $|N]^{(0)} = |n]^A|g]^B$ in which the solute is in the excited state n and the solvent is in the ground state g. Here, $|]^A$ and $|]^B$ denote ket vectors in the pure electronic spaces of the solute and the solvent, respectively. By applying the perturbation theory, the first-order total electronic state $|N]$ is approximated as

$$|N] \approx |n]^A\,|g]^B + \sum_{ng\neq et} |e]^A|t]^B \times \frac{[t|^B[e|^A H'|n]^A\,|g]^B}{\left(\varepsilon_n^A + \varepsilon_g^B\right) - \left(\varepsilon_e^A + \varepsilon_t^B\right)}, \tag{1}$$

where H' is the intermolecular interaction Hamiltonian whose physical nature is to be discussed later. ε_n^A, ε_e^A, ε_g^B, and ε_t^B are the eigen energies of the corresponding pure electronic states denoted by the indices. When the solute possesses several low lying electronic states e whose energies are close to one another, the relation $|\varepsilon_n^A - \varepsilon_e^A| \ll |\varepsilon_g^B - \varepsilon_t^B|$ holds for any solvent states t which are $t \neq g$. Thus, contributions from solvent excited states ($t \neq g$) are neglected in the summation. Since we are interested in how vibrations of the solvent perturb the solute electronic states, the interaction Hamiltonian H' is expanded into a Taylor series of the solvent normal coordinates Q_b^B to yield

$$|N] = |n]^A|g]^B + \sum_{n\neq e} |e]^A|g]^B \frac{[g|^B[e|^A H'^0|n]^A|g]^B}{\varepsilon_n^A - \varepsilon_e^A} + \sum_b \sum_{n\neq e} |e]^A|g]^B \frac{h_{en}^b}{\varepsilon_n^A - \varepsilon_e^A} Q_b^B + \cdots, \tag{2}$$

where

$$h_{en}^b = [g|^B[e|^A \left(\frac{\partial H'}{\partial Q_b^B}\right)_0 |n]^A|g]^B. \tag{3}$$

The first term is the zero-order term, and the second term represents a correction to the zero-order term where electronic states of the solute are coupled due to the interaction with nearby solvent at a fixed geometry. A similar term (without neglecting the contribution from the excited electronic states of solvent) has been used by Myers and Birge[23] to account for the solvation effect of β-carotene in solution on the oscillator strength of molecular electronic transition. The third term is the term that we focus in the present paper, which represents the mixing of solute electronic states due to the vibration of the nearby solvent, namely, solute/solvent intermolecular vibronic coupling. A similar term has recently been derived to estimate the magnitude of non-Condon intermolecular coupling in the dimer units of cyanobacterial light harvesting protein, C-phycocyanin.[24]

By assuming the electrostatic interaction as the origin of intermolecular vibronic coupling, the interaction Hamiltonian in Eq. (3) may be expanded into a multipole interaction series.[25,26] For the interaction between neutral molecules, we have

$$H' = H'^{(\mu\mu)} + H'^{(\mu\Theta)} + \cdots = \sum_{\alpha\alpha'} T_{\alpha\alpha'}^{(\mu\mu)} \mu_\alpha^A \mu_{\alpha'}^B + \sum_{\alpha\beta} T_{\alpha\beta}^{(\mu\Theta)} \left(\mu_\alpha^A \Theta_\beta^B + \Theta_\beta^A \mu_\alpha^B\right) + \cdots, \tag{4}$$

where μ and Θ are the dipole and traceless quadrupole moment operators, respectively, of the solute and the solvent (μ^A, Θ^A or μ^B, Θ^B, respectively). The subscripts α, $\alpha'(= 1z, 1x, 1y)$ and $\beta(= 20, 21c, 21s, 22c, 22s)$ denote the tensorial components of the multipole moments as they are defined by the regular spherical tensor notation[27,28] in their respective molecular fixed frame of axis. The regular spherical tensor notation is connected to the Cartesian tensor notation by the following relationship:[25]

$$\mu_{1z} = \mu_z,\ \mu_{1x} = \mu_x,\ \mu_{1y} = \mu_y, \tag{5a}$$

$$\Theta_{20} = \Theta_{zz},\ \Theta_{21c} = \frac{2}{\sqrt{3}}\Theta_{xz},\ \Theta_{21s} = \frac{2}{\sqrt{3}}\Theta_{yz}, \quad \Theta_{22c} = \frac{1}{\sqrt{3}}(\Theta_{xx} - \Theta_{yy}),\ \Theta_{22s} = \frac{2}{\sqrt{3}}\Theta_{xy}. \tag{5b}$$

The orientation factors $T_{\alpha\alpha'}^{(\mu\mu)}$ and $T_{\alpha\beta}^{(\mu\Theta)}$ are the functions of orientations and positions of molecule A and B of which explicit expressions are given in Appendix A. Note that the orientation factor between multipoles of ith and jth

rank is proportional to R^{-i-j-1}, where R is the distance between the coupled molecules. The contributions from higher-order multipole interactions may be neglected at a certain intermolecular distance or longer. In Eq. (4), only the terms with $i + j \leq 3$ or up to R^{-4} dependence is included. The first term is the dipole–dipole interaction and the second term gives the two dipole–quadrupole interactions where the origins of dipole and quadrupole moments are permuted among a solute-solvent pair.

By substituting the first term of Eq. (4) into Eq. (3), we obtain an expression for intermolecular vibronic coupling with dipole–dipole interaction,

$$h_{en}^{b(\mu\mu)} = \sum_{\alpha\alpha'} T_{\alpha\alpha'}^{(\mu\mu)} [e|^A \mu_\alpha^A |n]^A \left(\frac{\partial [g|^B \mu_{\alpha'}^B |g]^B}{\partial Q_b^B} \right)_0. \quad (6)$$

Here, the interaction term is expressed as a product of three quantities, namely, the orientation factor, the electronic transition dipole moment of solute, and the dipole moment derivative (also known as the vibrational transition dipole moment) of solvent in the ground state. The electronic and vibrational contributions to intermolecular vibronic coupling are thus segregated into the pure coordinate spaces of the solute and the solvent. The two transition dipole moments determine the electronic and vibrational properties of intermolecular vibronic coupling. The coupled electronic states of the solute must have the symmetries between which electronic dipole transition is allowed. The vibrational modes of solvent should possess non-vanishing vibrational transition dipole moments, in other words, they must be infrared active vibrations. Above all, the relative orientation of the interacting transition dipoles determines the overall magnitude of the coupling constant. We here note that although the orientation factor does not depend on normal coordinates, orientation dependence of $h_{en}^{b(\mu\mu)}$ does depend on normal coordinates because the direction of vibrational transition dipoles may differ by mode to mode even within a molecule. In short, each vibration may have its own favorable direction.

Similarly, by substituting the second term of Eq. (4) into Eq. (3), the intermolecular vibronic coupling through dipole–quadrupole interaction is formulated

$$h_{en}^{b(\mu\Theta)} = \sum_{\alpha\beta} T_{\alpha\beta}^{(\mu\Theta)} \left[[e|^A \mu_\alpha^A |n]^A \left(\frac{\partial [g|^B \Theta_\beta^B |g]^B}{\partial Q_b^B} \right)_0 + [e|^A \Theta_\beta^A |n]^A \left(\frac{\partial [g|^B \mu_\alpha^B |g]^B}{\partial Q_b^B} \right)_0 \right]. \quad (7)$$

The first term inside the square bracket consists of an electronic transition dipole moment of solute and a quadrupole moment derivative of solvent in the ground state. Through this term, the electronic states of solute are coupled by the vibrations of solvent that changes the ground state quadrupole moment. By considering symmetry, those vibrations indeed coincide with the Raman active vibrations with exception of isotropic totally symmetric modes. This similarity of selection rule arises from the fact that both quadrupole moment and polarizability are expressed by symmetric second rank tensors, and the exception arises from the additional property of the quadrupole moment tensor that it has no trace component.

In the second term inside the square bracket of Eq. (7), the dipole moment derivative of solvent appears again. Therefore, in addition to the dipole–dipole term, infrared active modes of solvent may promote coupling of solute electronic states through this term as well. The counterpart of the interaction is the electronic transition quadrupole moment of solute, which introduces a different electronic selection rule in the intermolecular vibronic coupling from that from the dipole–dipole coupling term.

By the substitution of higher-order multipole interaction terms, such as a dipole–octapole term, it is possible to show that even both IR and Raman inactive but HR active vibrations, which were conventionally classified as "dark" modes, may be intermolecular vibronic coupling active. However, the magnitude of such higher order terms diminishes rapidly due to the R^{-i-j-1} dependence of the orientation factor and may not be detectable. In fact, it will be shown in Sec. IV that the contribution from the multipole interaction terms higher than dipole–quadrupole interaction can be neglected in the present case of the β-carotene/solvent system.

B. Resonance HR scattering

The vibronic theory of resonance HR scattering is obtained by following the derivation given in our previous report.[14] We omit the detailed derivation in the present paper and only to recite the final result from the reference. According to the formulation made in the present paper, two minor changes are introduced: (1) The intermolecular vibronic coupling constant is replaced with the one given by Eq. (3); (2) solvent degree of freedom is added in the electronic coordinate space.

From our previous study on the excitation profiles of the enhanced solvent bands, the enhanced HR bands of solvent under current experimental condition are shown to be originated from the 1-0 resonance first order vibronic term of the hyperpolarizability tensor elements.[14] The relevant term with the present notation is as follows:

$$(I_{\mathrm{HR}})_{if} \propto |(B_1')_{if}|^2, \quad (8)$$

$$(B_1')_{if} = \sum_{mu,v} \sum_b F(\omega_0)(\varepsilon_n - \varepsilon_e)^{-1} (M_\lambda)_{gn} h_{ne}^b (M_\mu)_{em} (M_\nu)_{mg} \times (f|v)\left(v\middle|Q_b^B\middle|u\right)(u|i), \quad (9)$$

where

$$(M_\lambda)_{gn} \equiv [g|^B [g|^A R_\lambda |n]^A |g]^B, \quad (10)$$

and

$$F(\omega_0) = \{(\varepsilon_{mu} - \varepsilon_{gi} - \hbar\omega_0)(\varepsilon_{nv} - \varepsilon_{gi} - 2\hbar\omega_0 - i\Gamma_{nv,gi})\}^{-1}. \quad (11)$$

Here, ω_0 and Γ are the angular frequency of the incident electromagnetic field and the damping constant, respectively. $|\ )$ denotes ket vectors in the pure vibrational spaces. Indices m, e, n, and g refer to the adiabatic total electronic states in the excited states $|m]^A|g]^B$, $|e]^A|g]^B$, and $|n]^A|g]^B$ and that in the

ground state $|g]^A|g]^B$, respectively, and f, v, u, and i designate the adiabatic vibrational states which span over the combined spaces of solute and solvent nuclear degrees of freedom. Equation (9) represents HR transitions involving solvent normal modes in the presence of the molecular near-field effect where optically allowed two-photon transition $(M_\mu)_{em}(M_\nu)_{mg}$ (possibly $3A_g \leftarrow 1A_g$ or $2A_g \leftarrow 1A_g$) and optically allowed resonant one-photon transition $(M_\lambda)_{gn}$ ($1B_u \rightarrow 1A_g$) in the solute electronic manifold are coupled through intermolecular vibronic interaction h^b_{ne}. Substituting Eq. (6) into Eq. (9), we obtain hyperpolarizability element arising from the dipole–dipole interaction

$$
\begin{aligned}
(B'_1)_{if} = & \sum_{mu,v} \sum_{b} F(\omega_0)(\varepsilon_n - \varepsilon_e)^{-1} \\
& \times \sum_{\alpha} (M_\lambda)_{gn} [n|^A \mu^A_\alpha |e]^A (M_\mu)_{em} (M_\nu)_{mg} \\
& \times \sum_{\alpha'} T^{(\mu\mu)}_{\alpha\alpha'} \left(\frac{\partial [g|^B \mu^B_{\alpha'} |g]^B}{\partial Q^B_b} \right)_0 \\
& \times (f|v)\left(v\middle|Q^B_b\middle|u\right)(u|i). \qquad (12)
\end{aligned}
$$

Similarly, substituting Eq. (7) into Eq. (9) gives the one arising from the dipole–quadrupole interactions

$$
\begin{aligned}
(B'_1)_{if} = & \sum_{mu,v} \sum_{b} F(\omega_0)(\varepsilon_n - \varepsilon_e)^{-1} \\
& \times \Bigg[\sum_{\alpha} (M_\lambda)_{gn} [n|^A \mu^A_\alpha |e]^A (M_\mu)_{em} (M_\nu)_{mg} \\
& \times \sum_{\beta} T^{(\mu\Theta)}_{\alpha\beta} \left(\frac{\partial [g|^B \Theta^B_\beta |g]^B}{\partial Q^B_b} \right)_0 \\
& + \sum_{\beta} (M_\lambda)_{gn} [n|^A \Theta^A_\beta |e]^A (M_\mu)_{em} (M_\nu)_{mg} \\
& \times \sum_{\alpha} T^{(\mu\Theta)}_{\alpha\beta} \left(\frac{\partial [g|^B \mu^B_\alpha |g]^B}{\partial Q^B_b} \right)_0 \Bigg] \\
& \times (f|v)(v|\, Q^B_b \,|u)(u|i). \qquad (13)
\end{aligned}
$$

Because of the explicit incorporation of vibrational transition dipole as well as quadrupole moments in the expression of hyperpolarizability, not only the infrared active but also the Raman active but HR inactive vibrations of solvent are expected to be enhanced through the intermolecular vibronic coupling. Therefore, examining the symmetry species of the enhanced bands in detail will be a crucial test for the validity of our theory.

III. EXPERIMENTAL

A. Apparatus

A picosecond cw mode-locked Ti:sapphire oscillator (Spectra Physics, Tsunami) was used as the light source. The center wavelength, the repetition rate, and the typical pulse duration were 810 nm, 82 MHz, and 3 ps, respectively. The output of the oscillator was attenuated by a neutral density filter and focused into a sample solution contained in a quartz fluorescence cuvette by an achromatic lens. The 90° scattered HR light was collected by a camera lens and dispersed by a polychromator (Horiba Jobin Yvon, iHR-320), and detected by a liquid nitrogen cooled charge coupled device detector (Roper Scientific, Spec-10 2KB-EV/LN). Scattered incident radiation was eliminated by a dichroic filter placed in front of the entrance slit of the spectrometer. Excitation power at the sample point was 300 mW. We note that the quadratic response of the HR signals has been confirmed with the excitation power up to 300 mW. For each sample solution, averaging over 40 spectra with 180 s exposure was done followed by subtraction by a neat solvent spectrum acquired in the same manner. A fraction of the incident beam was separated and introduced into a β-barium borate crystal for second harmonic generation. The intensity of the fundamental and the second harmonic signal were simultaneously monitored during HR measurements and used for making correction for any fluctuation of pulse characteristics during exposure. Wavelength dependence of instrumental sensitivity was corrected. Because of the large chromatic aberration of the camera lens used for collecting HR scattering light, the spectral range suitable for quantitative discussion is limited only within the Raman shift from 300 cm^{-1} to 1800 cm^{-1}.

B. Samples

All-*trans*-β-carotene, benzene-h_6 (high-performance liquid chromatography grade), cyclohexane-h_{12} (spectroscopic grade), and tetrahydrofuran (high-performance liquid chromatography grade) were purchased from Wako Chemical Corp. and used as received. All-deuterated benzene-d_6 (D:99.5%) and cyclohexane-d_{12} (D:99.5%) were also commercially obtained from Cambridge Isotope Laboratories, Inc., and used as received. Set volume of a concentrated stock solution of β-carotene in tetrahydrofuran was transferred with a micropipette to a volumetric flask. The solvent, tetrahydrofuran, was evaporated completely before remaining β-carotene was redissolved into desired solvent. The final concentration of the sample solution was 1.1×10^{-4} M for both benzene-h_6 and benzene-d_6 solution, and 1.4×10^{-4} M for both cyclohexane-h_{12} and cyclohexane-d_{12} solutions. The sample preparation was carried out under deep red light in order to prevent the sample from undergoing photoisomerization.

C. Density functional calculation

All of the density functional theory calculations were performed using the Gaussian 03W program suite.[29] The optimized geometry and the normal mode of vibrations were determined analytically using the B3LYP/6-3111G(d,p) level of theory computations. All obtained vibrational frequencies were scaled by a factor of 0.98 to achieve better agreement with the observed frequencies. The ground state permanent dipole and traceless quadrupole moments were obtained from the single point calculations at optimized geometry under the same basis sets as those used in the vibrational frequency

calculations. The normal coordinate derivatives of dipoles (quadrupoles) were estimated from the change in the ground state permanent dipole (quadrupole) moments derived by the single point calculation under distorted molecular structures along the relevant normal coordinate.

IV. RESULTS AND DISCUSSION

A. Difference spectra

Resonance HR spectra of β-carotene in benzene-h_6 (a; red), in benzene-d_6 (a; blue), and their difference spectrum (b) are shown in Figure 1. The vertical axis of the difference spectrum is taken so that bands observed in the hydrogenated solution appear as positive peaks and those in the deuterated solution as negative. In the difference spectrum, numbers of positive and negative peaks are observed. HR bands of solute and the two-photon fluorescence background should be absent in the difference spectrum, since these signals are insensitive to the deuteration of solvent and thus are canceled out by subtraction. Therefore, all the bands in the difference spectrum are solely ascribed to the enhanced HR signals of solvents. Note that non-resonance HR bands from bulk solvents, which are roughly an order of magnitude smaller in intensity than the enhanced bands, have no effect on the difference spectra because they had been pre-subtracted from the solution phase spectra as described in Sec. III.

As is predicted by our vibronic theory incorporating dipole–dipole and dipole–quadrupole interactions, many of the infrared as well as Raman active vibrations of solvent are found in the difference spectrum. The most prominent band observed in the difference spectrum at 679 cm^{-1} for positive (and at 501 cm^{-1} for negative direction) is assigned to an infrared active vibration of benzene, which, in fact, is the most intense IR band in the finger print region. All the other infrared active vibrations 1481 and 1039 cm^{-1} (and 1334 and 814 cm^{-1} for -d_6) are also found in the difference spectrum with the relative intensities similar to those in the infrared absorption spectrum. In addition to the above-mentioned three IR active vibrations, numbers of peaks are found and assigned to Raman active vibrations of the solvent. A similar and more pronounced observation is made in the case of cyclohexane(-h_{12}/-d_{12}) solutions [Figs. 2(a) and 2(b)]. The assignments of the observed enhanced peaks in the two difference spectra are made by referring to infrared, Raman, and hyper-Raman spectra of corresponding neat solvents. Results are tabulated in Tables I and II. The symmetry species of each band is taken from the literature.[15–18] Note that the mutual exclusion rule holds between infrared active and Raman active vibrations (as well as between Raman active and HR active vibrations) due to the presence of inversion symmetry in benzene and cyclohexane. Therefore, there is little ambiguity in these assignments of the observed solvent vibrations.

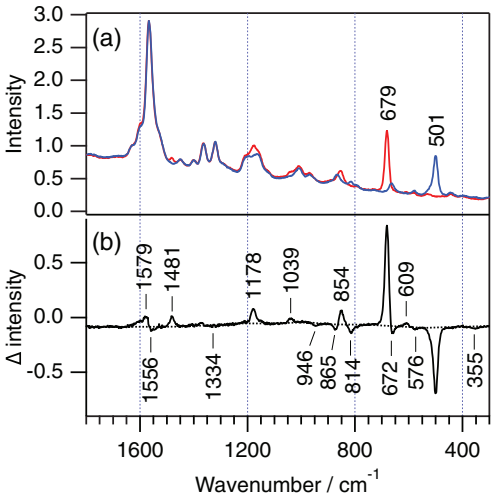

FIG. 1. Resonance HR spectra of all-trans-β-carotene (a) in benzene-h_6 (red) and in benzene-d_6 (blue), and their difference spectrum (b). Dotted line is an eye guide showing the baseline.

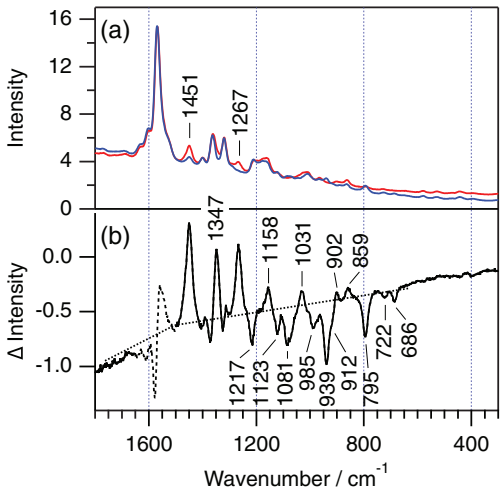

FIG. 2. Resonance HR spectra of all-trans-β-carotene (a) in cyclohexane-h_{12} (red) and in cyclohexane-d_{12} (blue), and their difference spectrum (b). Dotted line is the eye guide showing the baseline.

Here, we note that the relative intensities of the Raman active vibration in the difference HR spectrum are considerably different from those observed in the Raman spectrum; totally symmetric vibrations are generally prominent in the Raman spectrum but this is not the case with the HR difference spectrum. This tendency can be qualitatively explained by considering the traceless property of the quadrupole moment tensor. The well-known totally symmetric breathing mode of benzene, which gives a highly intense Raman band at 993 cm^{-1} (943 cm^{-1} for -d_6), is almost completely absent in the difference spectrum. Similar trend is found for the cyclohexane case where the strong Raman active totally symmetric mode at 802 cm^{-1} (723 cm^{-1} for -d_{12}) shows only weak intensities in the difference spectrum. These totally symmetric Raman bands are highly polarized and derive their intensities mostly from the isotropic part of the polarizability tensor. Generally speaking, these totally symmetric vibrations have the same symmetry with the isotropic part of a symmetric second rank tensor. Since quadrupole moment tensor is a symmetric second-rank tensor and does not have the isotropic part, those vibrations have little effect on the quadrupole moment derivatives that determine the activity in the intermolecular vibronic coupling.

TABLE I. Observed and reference vibrational frequencies of vibrational modes of benzene($-h_6$, $-d_6$), and their assignments.

Observed frequency (enhanced bands) (cm^{-1})		Reference frequency (neat solvent) (cm^{-1})		Assignment[a]	Sym. species[a]	Activity[b]		
$-h_6$	$-d_6$	$-h_6$[c]	$-d_6$[d]					
1579	1556	1586	1558	Ring stretch	e_{2g}		R	
1481	1334	1479	1330	Ring stretch + deform	e_{1u}	IR		HR
		1348	1056	CH/CD bend	a_{2g}			
		1310	1285	Ring stretch	b_{2u}			HR
1178	865	1177	868	CH/CD bend	e_{2g}		R	
		1149	824[a]	CH/CD bend	b_{2u}			HR
1039	814	1036	812	CH/CD bend	e_{1u}	IR		HR
		1011	970	Ring deform	b_{1u}			HR
		993	838	CH/CD bend	b_{2g}			
	946	993	945	Ring stretch	a_{1g}		R	
		973	795[a]	CH/CD bend	e_{2u}			HR
854	672	850	664	CH/CD bend	e_{1g}		R	
		702	600	Ring deform	b_{2g}			
679	501	676	500	CH/CD bend	a_{2u}	IR		HR
609	576	606	578	Ring deform	e_{2g}		R	
	355	403	352[a]	Ring deform	e_{2u}			HR

[a]Reference 15.
[b]IR, R, and HR refer to IR, Raman, and HR active vibrations, respectively.
[c]Reference 17.
[d]Reference 16 unless otherwise noted.

TABLE II. Observed and reference vibrational frequencies of vibrational modes of cyclohexane($-h_{12}$, $-d_{12}$), and their assignments.

Observed frequency (enhanced bands) (cm^{-1})		Reference frequency (neat solvent) (cm^{-1})		Assignments[a]	Sym. species[a]	Activity[b]		
$-h_{12}$	$-d_{12}$	$-h_{12}$[c]	$-d_{12}$[c]					
1451	1123	1466	1117	CH2/CD2 scis	a_{1g}		R	
1451	1081	1458	1069	CH2/CD2 scis	e_u	IR		HR
1451	1081	1458	1090	CH2/CD2 scis	a_{2u}	IR		HR
1451	1081	1445	1072	CH2/CD2 scis	e_g		R	
		1348	864[a]	CH2/CD2 twist	a_{1u}			HR
1347		1347	1163	CH2/CD2 wag	e_u	IR		HR
1347	795	1347	794	CH2/CD2 wag	e_g		R	
		1320	1126[a]	CH2/CD2 wag	a_{2g}			
1267	939	1268	937	CH2/CD2 twist	e_g		R	
1267	985	1261	991	CH2/CD2 twist	e_u	IR		HR
1158		1158	1012	CH2/CD2 rock	a_{1g}		R	
		1107	842[a]	CH2/CD2 wag	a_{1u}			HR
		1091	1187[a]	CC stretch + CC torsion	a_{1u}			HR
		1057	778[a]	CH2/CD2 twist	a_{2g}			
1031	912	1039	916	CH2/CD2 rock	a_{2u}	IR		HR
1031	1217	1029	1212	CC stretch	e_g		R	
902	686	906	686	CH2/CD2 rock	e_u	IR		HR
859	722	863	719	CC stretch	e_u	IR		HR
	722	802	723	CC stretch	a_{1g}		R	
		785	633	CH2/CD2 rock	e_g		R	
		522	393	CCC deform	a_{2u}	IR		HR
		423	372	CCC deform + CC torsion	e_g		R	
		384	298	CCC deform + CC torsion	a_{1g}		R	
		238	203[a]	CCC deform + CC torsion	e_u	IR		HR

[a]Reference 15.
[b]IR, R, and HR refer to IR, Raman, and HR active vibrations, respectively.
[c]Reference 18 unless otherwise noted.

Finally, the contribution of higher-order multipole interaction terms, such as a dipole-octapole term, is discussed. Benzene possesses five "dark" normal modes that are IR/Raman inactive but HR active in the wavenumber region lower than 1600 cm^{-1}. None of those bands, except for the weak one at 355 cm^{-1} in benzene-d_6, are observed in the difference spectrum. The absence of dark modes indicates negligible contribution from the higher-order multipole interaction, most probably due to the higher order inverse dependence on R.

B. Orientation analysis

In Sec. IV A, the selection rules of the enhanced solvent bands have been discussed. Next, we try to quantitatively analyze the observed enhanced solvent band intensity based on Eqs. (12) and (13). Analysis has been conducted in two steps. At first, a HR spectral pattern from a single solute-solvent pair at a selected geometry is calculated to investigate the orientational properties of the intermolecular vibronic coupling. Then, the theory is extended to cover a polymolecular system where a solute interacts with a number of solvent molecules.

Two assumptions are made in order to reduce the computational complexities. First, the initial state is assumed to be the vibrational ground state of the ground electronic state. Second, harmonic vibrational wave functions are assumed. Furthermore, in the case of solute with an inversion symmetry, as in the present β-carotene case, the second term in the square bracket in Eq. (13) vanishes because quadrupole transition between one-photon and two-photon allowed excited states are forbidden,

$$(M_\lambda)_{gn}[n|^A\Theta^A_\beta|e]^A(M_\mu)_{em}(M_\nu)_{mg} = 0. \tag{14}$$

As a result, the following interaction Hamiltonian is chosen:

$$h^b_{ne} = \sum_\alpha T^{(\mu\mu)}_{z\alpha}[n|^A\mu^A_z|e]^A\left(\frac{\partial[g|^B\mu^B_\alpha|g]^B}{\partial Q^B_b}\right)_0 + \sum_\beta T^{(\mu\Theta)}_{z\beta}[n|^A\mu^A_z|e]^A\left(\frac{\partial[g|^B\Theta^B_\beta|g]^B}{\partial Q^B_b}\right)_0. \tag{15}$$

Here, the direction of solute local frame of axis is taken so that transition dipole moment μ^A_{ne} is oriented parallel to the molecular fixed z-axis. Substituting Eq. (15) into Eq. (9) then into Eq. (8), HR intensity of a mode Q^B_b is given by

$$I_{\mathrm{HR}}(Q_b) \propto |G(\omega_0)|^2\left[\sum_\alpha T^{(\mu\mu)}_{z\alpha}\left(\frac{\partial[g|^B\mu^B_\alpha|g]^B}{\partial Q^B_b}\right)_0 + \sum_\beta T^{(\mu\Theta)}_{z\beta}\left(\frac{\partial[g|^B\Theta^B_\beta|g]^B}{\partial Q^B_b}\right)_0\right]^2 \times |(1_b|1_b)\langle 1_b|Q^B_b|0_b\rangle|^2, \tag{16}$$

$$G(\omega_0) = \sum_m F(\omega_0)(\varepsilon_n - \varepsilon_e)^{-1}(M_\lambda)_{gn}[n|^A\mu^A_z|e]^A \times (M_\mu)_{em}(M_\nu)_{mg}. \tag{17}$$

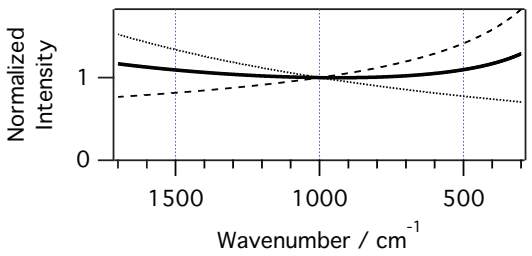

FIG. 3. Vibrational frequency dependence of $|G(\omega_0)|^2$ (dotted line), $|(1_b|Q_b|0_b)|^2$ (dashed line), and the product $|G(\omega_0)|^2|(1_b|Q_b|0_b)|^2$ (bold solid line). Curves are normalized at 1000 cm^{-1}.

A HR spectral pattern from a single solute-solvent pair at a given geometry can be calculated from Eq. (16) since numerical evaluation of the normal coordinate dependence of each quantity in the equation is possible. Under the harmonic oscillator approximation, the vibrational matrix element $|(1_b|Q_b|0_b)|^2$ yields a factor proportional to ω_b^{-1}, where ω_b is the frequency of the relevant vibration. A resonance electronic transition term $G(\omega_0)$ also exhibits normal coordinate dependence because each vibrational modes is in resonance to different vibronic states (1-0 resonance mechanism, see Ref. 14 for detail). ω_b dependence of $G(\omega_0)$ can be calculated based on the parameters determined by excitation profile measurements.[14] The ω_b dependence of these two factors are plotted in Fig. 3, in which ω_b dependence are shown to cancel with each other accidentally in the current region of interest to give almost ω_b independent plot for the product $|G(\omega_0)|^2|(1_b|Q_b|0_b)|^2$. The normal coordinate derivatives of dipoles and quadrupoles in Cartesian tensor formulation are estimated using the Gaussian 03W program suite.

Figure 4 shows calculated HR spectral patterns of the enhanced solvent vibrations of benzene with a fixed

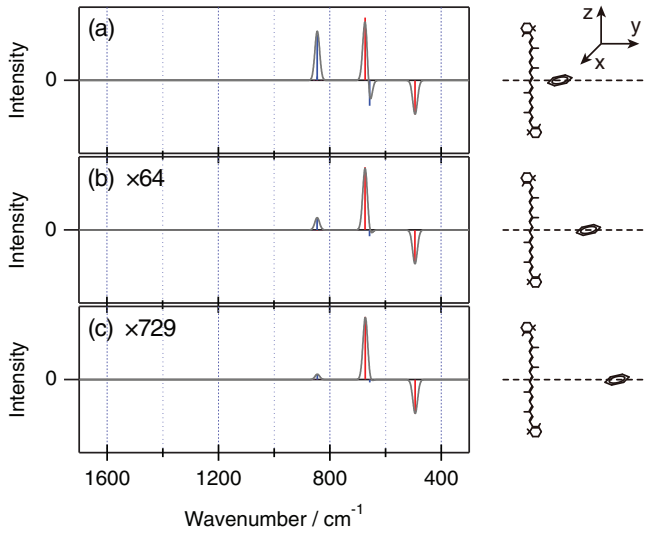

FIG. 4. Calculated HR spectral patterns of the enhanced solvent vibrations of benzene at intermolecular distances of 5 Å (a), 10 Å (b), and 15 Å (c). The corresponding relative geometries of the solvent with respect to solute are shown on the right side of each spectrum. Red and blue colored bars indicate the intensity of HR bands arisen from the dipole–dipole and dipole–quadrupole interactions, respectively. The solid gray curve shows the simulated overall difference spectra with artificial bandwidth of 20 cm^{-1}. Spectra in (b) and (c) are magnified by the factors designated in each graph.

geometry (see figure) at three different distances, 5, 10, and 15 Å. The bars indicate the intensities of individual normal modes, where red and blue colors correspond to bands arising from the dipole–dipole and dipole–quadrupole interactions, respectively. For a clear comparison with the observed spectra, the intensities of benzene-h_6 are plotted in the positive directions and those of benzene-d_6 are shown in the negative directions. The solid gray curve indicates the simulated overall difference spectra with artificial bandwidth of 20 cm^{-1} on each band. The simulated spectral patterns show comparable contributions from the dipole–dipole (red bar) and dipole–quadrupole induced (blue bar) HR bands, when the intermolecular distance R is 5 Å. When R is 15 Å, however, the red bar dominates the spectral pattern. This R dependence is not surprising since intensity of dipole–dipole induced vibrations follow R^{-6} dependence while dipole–quadrupole induced ones follow R^{-8}. It is interesting to obtain an R value close to the size of the first solvent shell (∼10 Å) in order to reproduce the observed relative intensity of bands arising from different multipole interactions. The results imply that the magnitude of quadrupole derivative of the solvent is, in fact, large enough to be able to give rise to the intermolecular vibronic coupling thorough interaction with the transition dipole of the solute.

The simulated spectral patterns also show drastic dependence on the solvent orientation with respect to the solute. Figure 5 shows calculated HR spectral patterns at a fixed distance (10 Å) with different orientations. The intensity of a particular vibrational mode increases when the molecular orientation is set to its favorable direction. This situation is best illustrated in Figs. 5(a)–5(c), where red bars (dipole–dipole interaction) show two distinct spectral patterns (a) and (b), (c). Since the interaction between two dipoles is maximized when they are aligned in the parallel geometry but vanishes when they are perpendicular to each other, the vibrational modes whose transition dipole moments pointing parallel to the z-axis of solute local axis are favored. It can be easily seen that only the out of plane vibration (679/501 cm^{-1}) gain large enhancement for the configuration (a), whereas, in contrast, only the in-plane vibrations (1481/1334, 1039/814 cm^{-1}) become prominent for the configurations (b) and (c). The blue bars (dipole–quadrupole interaction) follow different and more complicated orientation dependence. As a result, the enhanced bands exhibit characteristic spectral patterns on the relative orientation of the interacting molecule pairs.

Finally, we briefly discuss the effect of intermolecular distance R on the simulated HR spectral profiles. In contrast to the angular parameters which changes the spectral patterns greatly, R mainly governs the overall intensity as the intensity of dipole–dipole (red-bar) and quadrupole–dipole induced vibrations (blue bar) are proportional to R^{-6} and R^{-8}, respectively. When solvent is located at the apex of solute, where R ∼ 17 Å (Van der Waals radius of β-carotene (long axis) is estimated to be 14 Å[23] and that of benzene is 3 Å,[30,31] respectively), HR intensity is about 1–2 orders of magnitude smaller than when it is located alongside, where R ∼ 8 Å (Van der Waals radius of β-carotene (short axis) is estimated to be 5 Å[23] and that of benzene 3 Å, respectively),

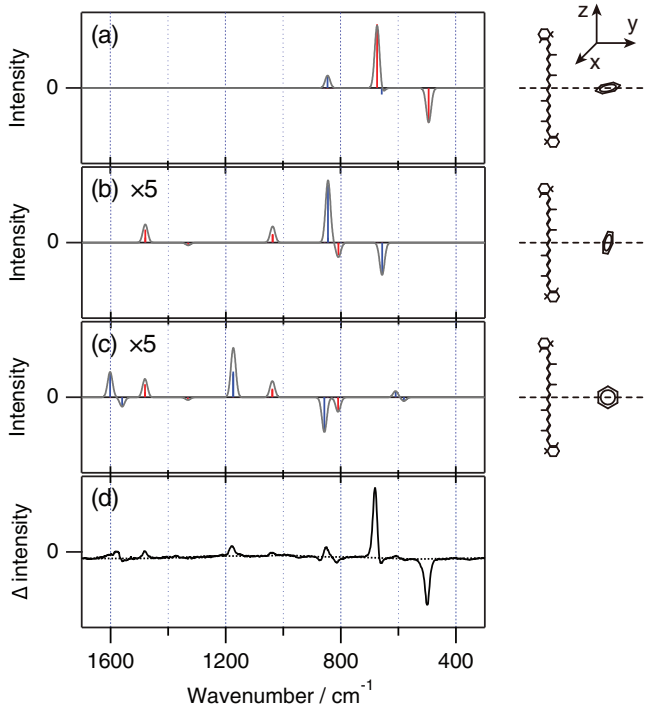

FIG. 5. Calculated HR spectral patterns of the enhanced solvent vibrations of benzene (a)–(c) and the observed difference spectrum in benzene solution (d). For the calculated spectra, a benzene molecule is placed with its ring plane parallel to xy (a), xz (b), and yz (c) plane of the solute local frame of axis. The corresponding relative geometries of the solvent with respect to solute are shown on the right side of each spectrum. Red and blue colored bars indicate the intensity of HR bands arisen from the dipole–dipole and dipole–quadrupole interactions, respectively. The solid gray curve shows the simulated overall difference spectra with artificial bandwidth of 20 cm^{-1}. Spectra in (b) and (c) are magnified by the factors designated in each graph. The intermolecular distance is set to 10 Å.

as expected from the doubled distance (2^{-6} = 1/64, 2^{-8} = 1/256).

So far, all the discussion has been based on a single solute-solvent pair. In order to account for the experimentally observed HR spectra, the theory must be extended to cover a polymolecular system where a solute can interact with more than one solvent molecule, since observed HR signal is generated from solutes that are surrounded by many solvent molecules. This is easily achieved by simply treating the interaction in N molecular system as a collection of N pairwise interactions because electrostatic interaction is strictly pairwise additive. In other words, one hyper-Raman transition accompanies only one vibrational transition of the solvent. The ergodicity assures that the rotational and translational motion of the molecules during the HR measurement is taken into account by taking ensemble average of the orientation factor in Eq. (16) over all the possible configurations of solute-solvent pairs when deriving the HR intensity

$$I_{\mathrm{HR}}(Q_b) \propto \frac{|G(\omega_0)|^2}{\omega_b}\left[\sum_{\alpha}\overline{\left|T_{z\alpha}^{(\mu\mu)}\right|^2}\left|\left(\frac{\partial[g|^B\mu_\alpha^B|g]^B}{\partial Q_b^B}\right)_0\right|^2 + \sum_{\beta}\overline{\left|T_{z\beta}^{(\mu\Theta)}\right|^2}\left|\left(\frac{\partial[g|^B\Theta_\beta^B|g]^B}{\partial Q_b^B}\right)_0\right|^2\right]. \quad (18)$$

Here, the overline ($\bar{}$) symbol denotes taking the ensemble average of the quantity under the bar. Because of the centrosymmetry of the solvent, benzene/cyclohexane, the dipole derivative, and quadrupole derivative are mutually exclusive, i.e., only either, if any, of the terms can have nonzero value for a normal mode Q_b^B. Therefore, the cross term is omitted when expanding the squared square bracket in Eq. (16).

In evaluating the ensemble average of the solvent configuration in the vicinity of solute, we adopt an approximation to further simplify the calculation. Although there are many solvent molecules surrounding the solute, the contribution from the solvent molecules with longer R may be neglected because the high order (6 or 8) inverse dependence of HR signal on R. Only the solvents in the first solvation shell at representative intermolecular distance R_0 is considered. Then, the following two extreme cases about the solvent orientation were compared: (1) A solute and the closest solvent molecules have a specific preferential orientation; (2) the solute and solvent molecule have no preferential orientation and can freely rotate around its center of inertia.

Simulated HR spectra for the above case 1 is the same as those shown in Figs. 4 and 5. Therefore, we can immediately conclude that the simulated HR spectra do not resemble the observed HR spectra, indicating unlikely presence of a specific preferential orientation in the solution.

In order to evaluate the case 2 where molecules can freely rotate around, i.e., random orientation, each orientation parameters were taken the rotational average over the relative orientation of solvent fixed local frame of axes. By taking the rotational average over solvent orientation (Appendix B)

$$\overline{\left|T_{z\alpha}^{(\mu\mu)}\right|^2} = \frac{1}{3}R_0^{-6}[3\overline{\cos^2\theta} + 1] \approx \frac{2}{3}R_0^{-6}, \tag{19a}$$

$$\overline{\left|T_{z\beta}^{(\mu\Theta)}\right|^2} = \frac{3}{5}R_0^{-8}[2\overline{\cos^2\theta} + 1] \approx R_0^{-8}, \tag{19b}$$

where θ is the polar angle in spherical coordinate designating the location of the solvent molecules on solute local coordinate system. Assuming the free rotation of solute gives the orientation average $\overline{\cos^2\theta} = 1/3$, yielding the last step in Eqs. (19a) and (19b). HR intensity (Eq. (18)) becomes

$$I_{\mathrm{HR}}(Q_b) \propto \frac{2}{3}R_0^{-6}\frac{|G(\omega_0)|^2}{\omega_b}\sum_\alpha\left|\left(\frac{\partial[g|^B\mu_\alpha^B|g]^B}{\partial Q_b^B}\right)_0\right|^2 + R_0^{-8}\frac{|G(\omega_0)|^2}{\omega_b}\sum_\beta\left|\left(\frac{\partial[g|^B\Theta_\beta^B|g]^B}{\partial Q_b^B}\right)_0\right|^2. \tag{20}$$

The HR signals from the same multipole interaction mechanism now have fixed spectral patterns because directionality of multipoles is averaged out. The intensity of each vibrational mode becomes proportional to the summed squared magnitude of the corresponding dipole/quadrupole transition moments, leaving R_0 as the only parameter to determine the whole HR spectral profile.

Figure 6 shows the comparison between the observed enhanced HR bands of benzene and the simulated difference spectrum after taking the rotational average of the solvent orientation. Figure 7 shows a similar comparison for the cyclohexane solution. Excellent agreement between the simulated HR spectra and the observed difference spectra in both solutions are achieved. Most of the characteristic features including the absence of strong totally symmetric Raman active vibrations mentioned earlier are reproduced in the simulated spectra. The result suggests that the presence of solute does not interfere solvent from freely rotating. The intermolecular distance to the nearest neighboring solvent are estimated to be roughly 10 Å from the simulation, which is in good agreement with the sum of van der Waals radii of the solute and solvents, indicating the possibility of efficient detection of the solvent molecules in the first solvation shell.

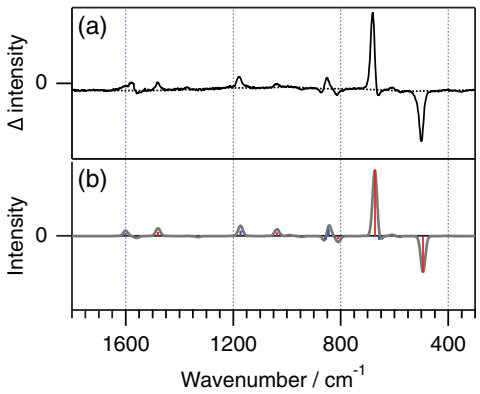

FIG. 6. Comparison of the observed (a) and simulated (b) difference HR spectra measured in benzene-h_6/-d_6 solutions. Simulated curves are calculated with the representative intermolecular distance R_0 of 10 Å.

So far, the experiments were conducted only for nonpolar solvents, because of the experimental difficulty arising from very poor solubility of β-carotene in polar solvents. However, we would like to emphasize that the theory should be equally applicable to the polar solvents, because the interaction Hamiltonian is based on the normal coordinate derivatives of the permanent dipoles/quadrupoles of the solvent but not on the permanent dipoles/quadrupoles themselves. Since the polar solvents are likely to form solvent structure due to permanent dipole–dipole interactions, specific solute–solvent orientation may exist. It would be of great interest, although

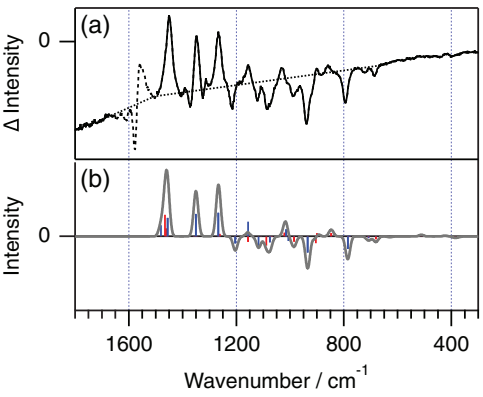

FIG. 7. Comparison of the observed (a) and simulated (b) difference HR spectra measured in cyclohexane-h_{12}/-d_{12} solutions. Simulated curves are calculated with the representative intermolecular distance R_0 of 10 Å.

challenging, to study the present molecular near-field effect in polar solvents.

C. General discussion

The present theory clearly indicates that the resonance HR molecular near-field effect is more rigorously interpreted as a photophysical response of a bimolecular system to an incident electromagnetic field. It can also be considered, however, as a resonant optical process of molecule *A* (β-carotene) that incorporates pairwise intermolecular interaction with nearby molecule *B* (benzene and cyclohexane). The transient electronic excitation of molecule *A* in this optical process may be regarded as a quasi-light source that acts on and detect molecule *B* in the near-field. The latter view is essentially the same as those discussed by Andrews and his co-workers[32,33] under the framework of quantum electrodynamics with virtual photon concept. It also better fits to the existing concept of near-field optics and spectroscopy. Here, we discuss two other analogous optical processes that may also be understood on the same basis.

Surface-Enhanced Raman/Hyper-Raman scattering (SEHRS)[34–37] and TERS[38–41] have apparent strong resemblance to the HR molecular near-field effect. They both require a probe (β-carotene in the present case and nanostructured metal in SERS). Incident laser wavelength must be tuned into the absorption of the probe. Observed enhanced Raman/HR spectra do not seem to follow the selection rules of conventional Raman scattering. When we first reported the HR signal enhancement by β-carotene in solution,[12,13] this resemblance lead us to introduce the term "molecular near-field effect," though at that time the origin of intensity enhancement was unclear. However, the present study has proved that its intensity enhancement mechanism is quite different from what is thought for SERS. The most widely accepted mechanism of SERS assumes the adsorbate Raman intensity enhancement by amplified electric field in the near-field of metal probe that is produced by the excitation of surface plasmon-polaritons.[34,42,43] In this electromagnetic mechanism, the interaction between probe and the adsorbate is not really essential for the Raman process. The field generated by the probe acts as if an external light source to the adsorbed molecule and hence it is possible to regard the whole process as a stepwise two independent optical processes; the excitation of surface plasmon-polaritons of the probe occurs first and Raman scattering of the adsorbate follows. On the other hand, in the HR molecular near-field effect, the transient electronic excitation acts as if a near-field antenna to let surrounding solvent's nuclear motion intrude into the resonance HR process of the probe molecule. The intermolecular interaction is embedded in the HR process, and it is not possible to further break down the whole process into two respective optical processes of the probe and the solvent. We note the possibility that, contrary to what is presently accepted, SERS/SEHRS and TERS should also be viewed as inseparable optical processes that arise from the molecular near-field effect.

Interaction between the two transition moments of nearby molecules during an optical process is also well-known as Fluorescence Resonance Energy Transfer, FRET.[44,45] In FRET, a photo excited donor molecule interacts with a nearby acceptor molecule in the ground state via a transition dipole-transition dipole interaction to create an excited state acceptor and a ground state donor, resulting in fluorescence emission from the acceptor molecule. Similar to the HR molecular near-field effect, intensity (or lifetime) of FRET signal shows large dependence on the relative geometries of interacting molecules owing to the large orientational dependence of the dipole–dipole interaction. Because of this property, FRET is known as a molecular ruler. The FRET process is considered as non-radiative energy transfer between donor and acceptor molecule during a fluorescence process.

There is a distinction to be discussed although the basic intermolecular interactions are similar for FRET and the molecular near-field effect. In FRET, electronic transitions take place between the real states of the molecules, hence the interacting transition dipole moments must be in resonance with each other, in other words, must connect states with the same amount of energy gap to satisfy energy conservation. This condition limits the FRET process to occur only among specific pairs of donor and acceptor molecules for which the emission spectrum of the former overlaps with the absorption of the latter. In the HR molecular near-field effect, the intermolecular energy transfer is not real, since there will be no net exchange of energy between the donor (molecule *A*) and the acceptor (molecule *B*). Although multipole interactions take place between these molecules, the energy for vibrational excitation of molecule *B* is provided via the intermediate states of molecule *A* by the electromagnetic field as the energy difference between the incident and scattered photon energies. Therefore, interactions can take place with a variety of vibrational transition dipole/quadrupole moments of the solvent irrespective of their transition energies. There is no restriction of the solvent molecule to be detected in the HR molecular near-field effect.

V. CONCLUSIONS

With the excellent reproduction of the observed spectra by the simulated spectra based on Eq. (20), we consider that the molecular level mechanism and the origin of the mysterious phenomenon, the "molecular near-field effect," has been fully elucidated. The origin of the effect is identified as an electromagnetic field generated by transient electronic excitation produced during the HR optical process. The excitation acts as if a near-field antenna to let surrounding solvent's nuclear motion intrude into the resonance HR process of β-carotene by way of dipole–dipole and dipole–quadrupole interactions. The intensity enhancement is well accounted for under the framework of resonance HR scattering where the solute "lend" its electronic resonance to the nearby solvent through the intermolecular vibronic coupling. The "molecular near-field effect" is more specifically termed as the "molecular near-field antenna effect."

The present study has shed light on a new type of optical process that specifically incorporates intermolecular interaction in the intermediate state. The selection rule in this optical

process is determined not only by the interactions with the incident electromagnetic field but also by the near-field multipolar intermolecular interactions. This class of optical processes may open up new possibilities of spectroscopy, molecular near-field spectroscopy, which provides direct observation methods of molecules lying in the vicinity of a molecular probe. We note the possibility that the SERS/SEHRS and TERS mechanism can also be explained on the same basis of molecular near-field antenna effect. With the use of Eq. (20), it is now possible to extract and discuss geometric information of solvating molecules around a solute with high molecular specificity characteristic of vibrational spectroscopy. It will be a powerful tool for investigating nanoscale intermolecular interactions in complex molecular systems.

ACKNOWLEDGMENTS

Part of this research has been supported by the National Science Council of Taiwan (NSCT) Grant No. NSC102-2113-M-009-003 and "Aiming to the Top University Project" of Ministry of Education in Taiwan. The authors are grateful to Professor S.-H. Lin for his insightful comments on intermolecular interactions.

APPENDIX A: DEFINITION OF ORIENTATION FACTORS

According to Ref. 25, the orientation factors in the spherical tensor formulation are defined as follows:

$$T^{(\mu\mu)}_{\alpha\alpha'} = R^{-3}\left(3r^A_\alpha r^B_{\alpha'} + c_{\alpha\alpha'}\right), \tag{A1}$$

$$T^{(\mu\Theta)}_{\alpha 20} = R^{-4}\frac{1}{2}\left[15\left(r^B_z\right)^2 r^A_\alpha + 6r^B_z c_{\alpha z} - 3r^A_\alpha\right], \tag{A2a}$$

$$T^{(\mu\Theta)}_{\alpha 21c} = R^{-4}\sqrt{3}\left[r^B_x c_{\alpha z} + c_{\alpha x} r^B_z + 5r^B_x r^B_z r^A_\alpha\right], \tag{A2b}$$

$$T^{(\mu\Theta)}_{\alpha 21s} = R^{-4}\sqrt{3}\left[r^B_y c_{\alpha z} + c_{\alpha y} r^B_z + 5r^B_y r^B_z r^A_\alpha\right], \tag{A2c}$$

$$T^{(\mu\Theta)}_{\alpha 22c} = R^{-4}\frac{\sqrt{3}}{2}\left\{5\left[\left(r^B_x\right)^2 - \left(r^B_y\right)^2\right]r^A_\alpha + 2r^B_x c_{\alpha x} - 2r^B_y c_{\alpha y}\right\}, \tag{A2d}$$

$$T^{(\mu\Theta)}_{\alpha 22s} = R^{-4}\sqrt{3}\left[5r^B_x r^B_y r^A_\alpha + r^B_x c_{\alpha y} + r^B_y c_{\alpha x}\right], \tag{A2e}$$

where

$$r^A_\alpha = \mathbf{e}^A_\alpha \cdot \mathbf{e}_{AB}, \quad r^B_{\alpha'} = \mathbf{e}^B_{\alpha'} \cdot \mathbf{e}_{BA} \quad \text{and} \quad r^B_{\alpha'} = \mathbf{e}^B_{\alpha'} \cdot \mathbf{e}_{BA} \tag{A3}$$

$\mathbf{e}^A_\alpha$ and $\mathbf{e}^B_{\alpha'}$ ($\alpha, \alpha' = x, y, z$) are the unit vectors defining the Cartesian local coordinate systems for the molecule A and B, respectively (Figure 8). $\mathbf{e}_{AB}$ and $\mathbf{e}_{BA}(= -\mathbf{e}_{AB})$ are unit vectors in the direction connecting the origins of local coordinates from A to B and from B to A, respectively. r^A_α and $r^B_{\alpha'}$ are projections of $\mathbf{e}_{AB}$ ($\mathbf{e}_{BA}$ in the case of latter) on local frame of axes of molecule A and B, respectively. $c_{\alpha\alpha'}$ corresponds to an element of rotation matrix which rotates $\mathbf{e}^A_\alpha$ into $\mathbf{e}^B_{\alpha'}$. We can write the following relationship:

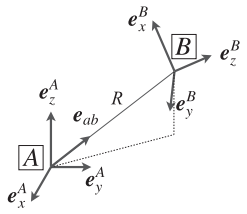

FIG. 8. The coordinate system of molecular frame of axes.

$$\mathbf{e}^B_{\alpha'} = \sum_i c_{i\alpha'}\mathbf{e}^A_i \tag{A4}$$

and thus,

$$r^B_{\alpha'} = \mathbf{e}^B_{\alpha'} \cdot \mathbf{e}_{BA} = -\sum_i c_{i\alpha'}\mathbf{e}^A_i \cdot \mathbf{e}_{AB} = -\sum_i c_{i\alpha'} r^A_i. \tag{A5}$$

APPENDIX B: ORIENTATION AVERAGE OF ORIENTATION FACTORS

We consider a problem of taking rotational average over the relative orientation of molecule B (solvent) fixed local frame of axes. Overline notation ($\bar{}$) for the quantity after the rotational average is introduced as follows:

$$\overline{f} = \frac{1}{8\pi^2}\int_0^\pi \int_0^{2\pi}\int_0^{2\pi} f(\Phi, \Psi, \Omega)\sin\Phi \mathrm{d}\Phi\mathrm{d}\Psi\mathrm{d}\Omega, \tag{B1}$$

where Euler angles Φ, Ψ, and Ω express the rotation of the molecule B fixed local frame of axes with respect to the molecule A fixed coordinate system.

1. Dipole–dipole interaction

By substituting Eq. (A5) into (A1), we obtain the expression for orientation factor of dipole–dipole interaction in terms of r^A_α and $c_{\alpha\alpha'}$ alone,

$$T^{(\mu\mu)}_{\alpha\alpha'} = R^{-3}\left(-3r^A_\alpha \sum_i c_{i\alpha'} r^A_i + c_{\alpha\alpha'}\right). \tag{B2}$$

Taking squared modulus, we get

$$\left|T^{(\mu\mu)}_{\alpha\alpha'}\right|^2 = R^{-6}\left[9\left(r^A_\alpha\right)^2 \sum_{i,j} c_{i\alpha'}c_{j\alpha'} r^A_i r^A_j - 6r^A_\alpha \sum_i c_{i\alpha'}c_{\alpha\alpha'} r^A_i + c_{\alpha\alpha'}c_{\alpha\alpha'}\right]. \tag{B3}$$

Taking the orientation average of both sides of the equation yields

$$\left\langle\left|T^{(\mu\mu)}_{\alpha\alpha'}\right|^2\right\rangle = R^{-6}\left[9\left(r^A_\alpha\right)^2 \sum_{i,j}\left\langle c_{i\alpha'}c_{j\alpha'}\right\rangle r^A_i r^A_j - 6r^A_\alpha \sum_i \left\langle c_{i\alpha'}c_{\alpha\alpha'}\right\rangle r^A_i + \left\langle c_{\alpha\alpha'}c_{\alpha\alpha'}\right\rangle\right]$$

$$= R^{-6}\left[9\left(r_\alpha^A\right)^2 \sum_{i,j} \frac{\delta_{ij}}{3} r_i^A r_j^A - 6 r_\alpha^A \sum_i \frac{\delta_{i\alpha}}{3} r_i^A + \frac{1}{3}\right]$$

$$= R^{-6}\left[3\left(r_\alpha^A\right)^2 \sum_i \left(r_i^A\right)^2 - 2\left(r_\alpha^A\right)^2 + \frac{1}{3}\right]. \quad \text{(B4)}$$

Notice that r_α^A are independent of Euler angles Φ, Ψ, and Ω, thus, are invariant under rotational average. When deriving the second line, the following property of the rotational averages of direction cosine is used[46]

$$\langle c_{i\alpha} c_{j\alpha} \rangle = \frac{\delta_{ij}}{3}, \quad \text{(B5)}$$

where δ_{ij} is the Kronecker delta function. Substituting the equality

$$\sum_i \left(r_i^A\right)^2 = 1, \quad \text{(B6)}$$

Eq. (B1) is simplified to

$$\left\langle \left| T_{\alpha\alpha'}^{(\mu\mu)} \right|^2 \right\rangle = R^{-6}\left[\left(r_\alpha^A\right)^2 + \frac{1}{3}\right]. \quad \text{(B7)}$$

Defining polar θ and azimuthal ϕ angles in the spherical coordinate designating the location of the solvent molecules on solute local coordinate system,

$$r_x^A = \sin\theta\cos\phi, \quad r_y^A = \sin\theta\sin\phi, \quad \text{and} \quad r_z^A = \cos\theta. \quad \text{(B8)}$$

The z-component of the orientation factor is derived,

$$\left\langle \left| T_{z\alpha'}^{(\mu\mu)} \right|^2 \right\rangle = R^{-6}\left[\cos^2\theta + \frac{1}{3}\right]. \quad \text{(B9)}$$

2. Dipole–quadrupole orientation factor

Orientation average of the orientation factors of dipole–quadrupole interaction can be calculated in the same manner as dipole–dipole interaction. All five factors results in the exact same expression,

$$\left\langle \left| T_{z\beta}^{(\mu\Theta)} \right|^2 \right\rangle = \frac{3}{5} R^{-8}\left[2\left(r_z^A\right)^2 + 1\right] = \frac{3}{5} R^{-8}[2\cos^2\theta + 1]. \quad \text{(B10)}$$

In the above derivation, the following relationships are used in addition to Eq. (B5):[46]

$$\langle c_{i\alpha} c_{j\alpha} c_{k\alpha} c_{l\alpha} \rangle = \frac{\delta_{ij}\delta_{kl} + \delta_{ik}\delta_{jl} + \delta_{il}\delta_{jk}}{15}, \quad \text{(B11)}$$

$$\langle c_{i\alpha} c_{j\alpha} c_{k\beta} c_{l\beta} \rangle = \frac{4\delta_{ij}\delta_{kl} - \delta_{ik}\delta_{jl} - \delta_{il}\delta_{jk}}{30}. \quad \text{(B12)}$$

[1] R. Terhune, P. Maker, and C. Savage, Phys. Rev. Lett. **14**, 681 (1965).
[2] S. J. Cyvin, J. E. Rauch, and J. C. Decius, J. Chem. Phys. **43**, 4083 (1965).
[3] D. A. Long and L. Stanton, Proc. R. Soc. London, Ser. A **318**, 441 (1970).
[4] D. A. Long, M. French, T. J. Dines, and R. Hall, J. Phys. Chem. **88**, 547 (1984).
[5] J. H. Christie and D. J. Lockwood, J. Chem. Phys. **54**, 1141 (1971).
[6] D. Andrews and T. Thirunamachandran, J. Chem. Phys. **68**, 2941 (1978).
[7] D. Andrews and T. Thirunamachandran, J. Chem. Phys. **70**, 1027 (1979).
[8] K. Altmann and G. Strey, J. Raman Spectrosc. **12**, 1 (1982).
[9] V. Denisov, B. Mavrin, and V. Podobedov, Phys. Rep. **151**, 1 (1987).
[10] L. D. Ziegler, J. Raman Spectrosc. **21**, 769 (1990).
[11] A. M. Kelley, Annu. Rev. Phys. Chem. **61**, 41 (2010).
[12] R. Shimada, H. Kano, and H. Hamaguchi, J. Raman Spectrosc. **37**, 469 (2006).
[13] R. Shimada, H. Kano, and H. Hamaguchi, J. Chem. Phys. **129**, 024505 (2008).
[14] R. Shimada and H. Hamaguchi, J. Chem. Phys. **134**, 034516 (2011).
[15] T. Shimanouchi, *Tables of Molecular Vibrational Frequencies Consolidated* (National Bureau of Standards, USA, 1972), Vol. I, pp. 1–164.
[16] J. Bertie and C. Keefe, Fresenius J. Anal. Chem. **362**, 91 (1998).
[17] J. Bertie and C. Keefe, J. Mol. Struct. **695**, 39 (2004).
[18] E. Matrai, P. Csaszar, G. Fogarasi, and M. Gal, Spectrochim. Acta A **41**, 425 (1985).
[19] Y. Chung and L. D. Ziegler, J. Chem. Phys. **88**, 7287 (1988).
[20] V. Petrov, Opt. Spektrosk. **59**, 1315 (1985).
[21] J. Neddersen, S. Mounter, J. Bostick, and C. Johnson, J. Chem. Phys. **90**, 4719 (1989).
[22] V. Petrov, Opt. Spektrosk. **59**, 469 (1985).
[23] A. B. Myers and R. Birge, J. Chem. Phys. **73**, 5314 (1980).
[24] J. M. Womick, B. A. West, N. F. Scherer, and A. M. Moran, J. Phys. B **45**, 154016 (2012).
[25] A. J. Stone, *The Theory of Intermolecular Forces* (Oxford University Press, 1997).
[26] J. O. Hirschfelder, C. F. Curtiss, and R. B. Bird, *Molecular Theory of Gases and Liquids* (Wiley-Interscience, 1964) (revised edition).
[27] R. N. Zare, *Angular Momentum: Understanding Spatial Aspects in Chemistry and Physics* (Wiley-Interscience, 1988).
[28] D. M. Brink and G. R. Satchler, *Angular Momentum*, 3rd ed. (Oxford University Press, New York, 1993).
[29] M. J. Frisch, G. W. Trucks, H. B. Schlegel *et al.*, GAUSSIAN 03, Revision B.04, Gaussian, Inc., Wallingford, CT, 2004.
[30] A. H. Narten, J. Chem. Phys. **67**, 2102 (1977).
[31] Z. Bochynski and H. Drozdowski, Acta Phys. Slovaca **49**, 409 (1999).
[32] D. L. Andrews and N. P. Blake, J. Mod. Opt. **37**, 701 (1990).
[33] D. L. Andrews and P. Allcock, Chem. Soc. Rev. **24**, 259 (1995).
[34] D. L. Jeanmaire and R. P. Van Duyne, J. Electroanal. Chem. Interfacial Electrochem. **84**, 1 (1977).
[35] M. G. Albrecht and J. A. Creighton, J. Am. Chem. Soc. **99**, 5215 (1977).
[36] M. Fleischmann, P. J. Hendra, and A. J. McQuillan, Chem. Phys. Lett. **26**, 163 (1974).
[37] *Surface-Enhanced Raman Scattering*, edited by K. Kneipp, M. Moskovits, and H. Kneipp (Springer, Berlin, 2006).
[38] R. M. Stöckle, Y. D. Suh, V. Deckert, and R. Zenobi, Chem. Phys. Lett. **318**, 131 (2000).
[39] N. Hayazawa, Y. Inouye, Z. Sekkat, and S. Kawata, Opt. Commun. **183**, 333 (2000).
[40] M. S. Anderson, Appl. Phys. Lett. **76**, 3130 (2000).
[41] B. Pettinger, G. Picardi, R. Schuster, and G. Ertl, Electrochemistry (Tokyo) **68**, 942 (2000).
[42] H. Xu, E. Bjerneld, M. Käll, and L. Börjesson, Phys. Rev. Lett. **83**, 4357 (1999).
[43] H. Xu, J. Aizpurua, M. Käll, and P. Apell, Phys. Rev. E **62**, 4318 (2000).
[44] T. Förster, Ann. Phys. **437**, 55 (1948).
[45] J. R. Lakowicz, *Principles of Fluorescence Spectroscopy*, 3rd ed. (Springer US, Boston, MA, 2006).
[46] D. A. Long, *The Raman Effect* (John Wiley & Sons, Ltd., Chichester, UK, 2002), pp. 355–358.